Shear-thinning Nanocomposite Hydrogels for the Treatment of Hemorrhage

Akhilesh K. Gaharwar, Reginald K. Avery, Alexander Assmann, Arghya Paul, Gareth H. McKinley, Ali Khademhosseini*, Bradley D. Olsen*

*Prof. B. D. Olsen, Dr. A. K. Gaharwar
Department of Chemical Engineering, Massachusetts Institute of Technology, Cambridge, MA 02139 (USA)
Email: (bdolsen@mit.edu)

*Prof. A. Khademhosseini, Dr. A. K. Gaharwar, Dr. A. Assmann, Dr. A. Paul
Wyss Institute for Biologically Inspired Engineering, Harvard University,
Boston, MA 02115 (USA)
Email: (alik@rics.bwh.harvard.edu)

Prof. A. Khademhosseini, Dr. A. K. Gaharwar, R. K. Avery, Dr. A. Assmann, Dr. A. Paul
Center for Biomedical Engineering, Department of Medicine, Brigham and Women's Hospital, Harvard Medical School, Cambridge, MA 02139 (USA)

Prof. A. Khademhosseini, Dr. A. K. Gaharwar, Dr. A. Assmann, Dr. A. Paul
Harvard-MIT Division of Health Sciences and Technology, Massachusetts Institute of Technology, Cambridge, MA 02139 (USA).

Dr. A. K. Gaharwar
David H. Koch Institute for Integrative Cancer Research, Massachusetts Institute of Technology, Cambridge, MA 02139 (USA)

R. K. Avery
Department of Biological Engineering, Massachusetts Institute of Technology, Cambridge, MA 02139 (USA)

Prof. G. H. McKinley
Department of Mechanical Engineering, Massachusetts Institute of Technology, Cambridge, MA 02139 (USA)

Dr. A. Assmann
Department of Cardiovascular Surgery, Heinrich Heine University, Medical Faculty, 40225 Duesseldorf (Germany)

Shear-thinning Nanocomposite Hydrogels for the Treatment of Hemorrhage

Internal hemorrhaging is a leading cause of death after traumatic injury on the battlefield. Although several surgical approaches such as the use of fibrin glue and tissue adhesive have been commercialized to achieve hemostasis, these approaches are difficult to employ on the battlefield and cannot be used for incompressible wounds. Here, we present shear-thinning nanocomposite hydrogels composed of synthetic silicate nanoplatelets and gelatin as injectable hemostatic agents. These materials are demonstrated to decrease *in vitro* blood clotting times by 77 %, and shown to form stable clot-gel systems. *In vivo* tests indicated that the nanocomposites are biocompatible and capable of promoting hemostasis in an otherwise lethal liver laceration. The combination of injectability, rapid mechanical recovery, physiological stability, and the ability to promote coagulation result in a new hemostat for treating incompressible wounds in out-of-hospital, emergency conditions.

A range of hemostats have been reported that decrease the time required to establish hemostasis by dehydrating the injury site,[1, 2] concentrating clotting factors,[2, 3] delivering clotting agents (such as thrombin and fibrinogen)[1, 2, 4] or forming a physical barrier against bleeding,[5] to the injured site to promote clotting. However, most of these hemostats are suitable for external wounds,[6, 7] where hemostatic agents and external pressure can be applied simultaneously. Recently, thrombin and fibrinogen-based injectable solutions have been developed, but these injectable solution-based hemostats pose the risk of introducing strong coagulation activators into the circulatory system.[8, 9] Therefore, there is a need for new hemostatic biomaterials that are injectable into a wound, mechanically stable, and induce rapid and local hemostasis.

One approach to developing hemostatic agents for traumatic injuries is to engineer injectable biomaterials that can be introduced into a wound site, forming a physiologically stable artificial matrix and promoting the natural clotting cascade. Specifically, the biomaterial should flow with minimal applied pressure during injection, providing a method of application that avoids additional patient trauma. However, once in the wound, the material should solidify to prevent biomaterial loss to unaffected areas. Shear-thinning hydrogels can satisfy these requirements and have been developed from a wide variety of material platforms.[10, 11]

Multiple approaches have been developed to incorporate functional materials into hemostats to enhance their therapeutic properties. These include commercial products such as QuikClot™ that incorporate kaolin, a crystalline mineral that functions as an absorbent and coagulation activator.[12] Floseal® uses gelatin and thrombin to promote clotting in an injectable form.[8] An emerging approach to integrate functionality into hydrogel networks focuses on incorporating nanoparticles.[13, 14, 15, 16, 17] Nanomaterials have been shown to interact with blood to promote clotting via mechanisms such as platelet activation, dehydration of the plasma, delivery of coagulating factors, formation of physical barriers, or the activation of clotting factors.[1, 18, 19, 20, 21, 22]

Highly charged nanoparticles, such as synthetic silicate nanoplatelets, have been shown to induce blood coagulation by concentrating clotting factors.[4] Synthetic silicates are charged disks, 20-30 nm in diameter and ~1 nm in thickness.[23] Due to the anisotropic distribution of their surface charge, positive along the edge and negative on the top and bottom surfaces, the nanoplatelets can form self-assembled structures which can dynamically form and break, creating shear thinning gels when in aqueous media.[24] Recently, synthetic silicate nanoplatelets have been used as osteogenic agents,[23] drug delivery agents,[25] tissue engineered scaffolds,[26, 27,

[28, 29] solid hemostat products,[4, 30, 31] additives in cosmetic creams,[32, 33] and rheological modifiers.[34] Synthetic silicates such as Laponite are shown to degrade into non-toxic components (Na^+, Mg^{2+}, $Si(OH)_4$, Li^+) in physiological conditions.[35] Moreover, these silicates are found to be cytocompatible with human stem cells and animal cells as reported in previous literature.[23, 26, 28]

Natural and synthetic polymers have been shown to interact with synthetic silicates through physical interactions, forming physically crosslinked networks.[26, 28, 29, 36, 37] Earlier studies on silicate-gelatin interactions show that polyampholytic gelatin, containing positive and negative regions, strongly interacts with the oppositely charged areas of the synthetic silicate nanoplatelets.[38] Gelatin is denatured collagen, and mimics components of the native extracellular matrix (ECM) in structure and chemical composition.[39] Gelatin's hygroscopic property also allow for absorption of body fluids and is proposed for a range of tissue engineering applications.

Physical mixtures of gelatin and silicate nanoplatelets were used to formulate the nanocomposite hydrogels for this study. Briefly, the silicate nanoplatelets were exfoliated in ultrapure (Milli-Q) water using a vortexer to enhance the surface area available for interaction with gelatin. Next, a gelatin stock, heated to liquefy the solution, was vigorously mixed with the exfoliated silicate at room temperature (**Figure 1a**). Vigorous agitation was necessary to prevent clumping of the nanoplatelets during gelation; however, the nanoplatelets are stably dispersed after the gel has set.[24] Nanocomposite hydrogels were fabricated with solid concentrations of 3, 6, and 9 wt% and gelatin:nanoplatelet ratios from 0:1 to 1:0 and labeled as xNCy ("x" represents the total solid weight percent and "y" is percent of the total solid weight percent that is nanoplatelet) (**Supplementary Table 1**). Initially the gelatin solution was a viscous liquid (at 37 ^oC), but once silicate nanoplatelets were mixed with gelatin, the solution gelled within a minute.

When mixed with gelatin, silicate nanoplatelets improved the thermal stability of the hydrogel. Thermal stability of the nanocomposite formulations was determined by oscillatory shear rheology over a temperature range from 15 °C to 45 °C, mimicking common environmental and physiological temperatures that the nanocomposite may be exposed during sample preparation and *in vivo* application. 9NC0 had a gel-sol transition temperature of 32 °C (**Supplementary Figure 1**), consistent with the literature and too low for application as a hemostat.[40] However, the addition of silicate nanoplatelets to gelatin improved the thermal stability, increasing the sol-gel transition to above 45 °C for solids concentrations of 6 wt% or greater. In contrast, 3 wt% solids nanocomposites were not solid within the experimentally observed temperature range. For treatment of hemorrhage, thermal stability is necessary once the nanocomposite is injected so that it can remain at the wound site without flowing into adjacent areas. Similarly, physiological stability was observed for all 9 wt% nanocomposites, 6NC50, 6NC75, and 6NC100 (**Supplementary Figure 2**). All gelatin samples, quickly dissolved in PBS at 37 °C while the aforementioned samples had no observed weight loss over 24 hours. For this reason, only nanocomposite hydrogels with more than 6 wt% solids were characterized further.

Zeta potential measurements suggest that electrostatic interactions between nanoplatelets and gelatin contributed to the observed increase in the thermal stability (**Figure 1b**). Solutions of silicate nanoplatelets possessed a zeta potential of -39 mV, whereas gelatin solutions had a zeta potential of 10 mV. Because the two components had opposite charges, electrostatic interactions between silicate and gelatin were expected. This was also supported by earlier findings which showed that strong interactions between montmorillonite (another type of silicate clay) and gelatin can function to increase the sol-gel transition temperature of the composite.[41]

Scattering measurements of nanocomposite hydrogels suggest the presence of disk shaped particles, indicating that clay particles remain exfoliated in the nanocomposite. Small angle X-ray scattering (SAXS) intensity curves of the nanocomposites showed power law decay with an exponent of -2 at high q, the scattering vector, characteristic of disk-shaped scatterers. The scattering intensity from 9NC75 can be fit with a thin disk model with a radius of 9.5±2.7 nm, in agreement with the reported size of the silicate nanoplatelets (**Figure 1c**).[23] This suggests that scattering was produced from individual nanoplatelets dispersed within the gelatin in this formulation and not aggregates of nanoplatelets (**Supplementary Figure 3**).

Silicate addition to gelatin modulated the rheological response of the nanocomposite, resulting in a shear yielding behavior observed at 37 °C. Preliminary investigations using a 22-gauge needle indicated that all silicate-containing nanocomposite hydrogels could be injected and form self-supporting structures, suggesting the presence of a yield stress and recovery potential (**Figure 1a**). Linear oscillatory shear rheology showed that the crossover frequency was below 0.001 Hz for 9NC75 and 9NC100, maintaining solid-like (G'>G'') properties over the tested frequency range (**Supplementary Figure 4**). Oscillatory strain into the non-linear regime (**Supplementary Figure 4**) illustrated yielding behavior, an important parameter for designing hydrogels for minimally invasive therapies. In oscillatory shear rate sweeps, the yield stress was defined as a 5% departure of the stress from the initial linearity on a stress-strain plot. Tests were performed at 37 ºC, where gelatin readily flows and lacks a yield stress (**Figure 1d & S4**). An increase in the silicate concentrations from 0% (9NC0) to 100% (9NC100) increased the yield stress from 2 Pa to 89 Pa. A yield stress was observed in 9NC100 but not in 9NC0, suggesting that the yield stress behavior was derived from the presence of the dispersed nanoplatelets in the nanocomposite, consistent with the known shear thinning capability of

nanoplatelets.[40] Because increasing concentration of gelatin reduces the yield stress, it eases delivery of the nanocomposite by injection.

Recovery of the elastic gel strength in less than 10 seconds was observed in nanocomposites for nanoplatelet loadings greater than 50% (9NC50, 9NC75, and 9NC100). Such rapid self-healing after the removal of stress can prevent material flow after application to a wound site. This provides a significant advantage over self-assembling peptides, which risk being washed away because they have relatively long self-healing times after the deformation of physically crosslinked networks.[5] **Figure 1e** shows four cycles of high (100%) to low (1%) oscillatory strain amplitudes and the resulting nanocomposite moduli. These results indicate rapid recovery of the storage modulus after repeated application of high oscillatory strain amplitudes, suggesting rapid recovery of the physically crosslinked networks. After four cycles of high and low oscillatory strain, the 9NC50 modulus observed during large amplitude strain oscillations was 80% lower than the initial modulus. At higher silicate loading (9NC75 and 9NC100), the moduli were 33% and 29% lower compared to the initial values. Extended monitoring (**Supplementary Figure 5**) indicated that after 30 seconds the moduli reached asymptotic values, indicating completion of the healing process.

The incorporation of silicate nanoplatelets into gelatin led to a decrease in the observed clotting time *in vitro*. The hemostatic ability of nanocomposite hydrogels was evaluated by monitoring the clotting time of whole blood in contact with the nanocomposite surfaces in 96-well plates. Under normal conditions, human blood coagulates in 5-6 minutes.[4, 42] Similar clotting times (5.2±0.5 minutes) for whole blood were observed in control wells containing neither gelatin nor nanocomposite (**Figure 2a and 2b**). A slight color change was observed 9NC0 by 5 minutes. This was attributed to the tamponade ability of gelatin.[43] Gelatin is

hygroscopic and could absorb the fluid components of whole blood but could not stimulate clot formation within 5 minutes. The addition of nanoplatelets to gelatin reduced blood clotting time in a dose-dependent manner. **Figure 2a and 2b** demonstrate the decreased clotting time for higher nanoplatelet concentrations. 9NC25, 9NC50 and 9NC75 reduced the clotting time by 32%, 54%, and 77%, respectively when compared to the control (blood in uncoated wells). The representative images of wells at select time points, shown in **Figure 2a**, clearly highlight the presence of a clot earlier in nanocomposites with higher nanoplatelet loadings. This was attributed to the strong negative charge of the synthetic silicate nanoplatelet that can facilitate concentration of clotting factors near the nanocomposite surface. Prior studies have shown a decrease in clotting time due to the addition of negatively charged particles to polymer hydrogels.[4, 12] Preliminary *in vitro* studies indicate that the nanocomposites induced minimal cytotoxic effect or inflammatory response (**Supplementary Figure 6**), with gelatin-containing nanocomposites having higher cell viability and lower inflammatory response than NC100 gels, supporting the potential application of these materials as biocompatible hemostatic gels.

Decreased clotting times of blood in contact with nanocomposites were also observed through rheological measurements. Small amplitude oscillatory time sweeps of blood in contact with gelatin or gelatin-silicate nanocomposites were performed to evaluate clotting kinetics (**Figure 2c**). Clotting induced an increase in the elastic modulus of the gelatin-clot system from 10^{-1} to 10^{4} Pa (**Figure 2c**). Whole blood in contact with gelatin clotted in 5-7 minutes, which is consistent with our earlier clotting data and the literature.[44] When gelatin was replaced with a silicate-gelatin nanocomposite, the clotting transition occurred even prior to the initiation of measurements, reflecting a large reduction in the clotting time. Comparing the decrease in clotting time observed with nanocomposites to other reported hemostatic products, the

improvement exceeds many solid hemostats and was similar to recorded values for thrombin-based hemostats (**Figure 2d**). [4, 6, 44, 45] A comparison of the nanocomposite and the commercial hemostat QuikClot™ clot mass per contact area as a function of time showed similar trends in clot formation (**Supplementary Figure 7**).

Blood clot strength was preserved in blood-nanocomposite systems. Clot strength, characterized by the peak shear stress attained in a linearly increasing strain experiment, is a parameter important for establishing hemostasis. More rigid clots are more likely to embolize while more pliable clots are ineffective. Stress-strain curves of each system were compared to a natural clot under the same testing conditions. The results indicate that the clot could sustain a peak shear stress of 2.4±0.3 kPa, while the gelatin-clot system had a peak shear stress of 0.5 kPa (**Supplementary Figure 8**). The liquid-like properties of gelatin (G''>G') at 37 °C compromise the mechanical stability of the system. Nanocomposites tested under the same conditions reached a maximum shear stress of 1.0±0.09 kPa. In the presence of nanocomposite, the shear stress of a nanocomposite-clot was 1.9±0.6 kPa, which is comparable to the peak stress borne by the clot. It was hypothesized that the surface charge of the nanocomposite facilitated platelet aggregation or activation of clotting factors that ultimately enhanced the hemostatic activity. To confirm this, a channel was generated within the nanocomposite hydrogels and subsequently filled with blood. It was observed that platelets aggregated near the nanocomposite surface (**Supplementary Figure 9**), which was not observed in control experiments on gelatin or plastic surfaces. This indicates that nanocomposite surfaces might be effective in attracting blood components.

Observations in the presence of platelet rich plasma (PRP) and platelet poor plasma (PPP) (**Supplementary Figure 9**) indicated that components in both plasma types were co-localized with silicates, forming aggregates around the silicates. This co-localization and protein

adsorption to the nanocomposite surfaces could be driven by electrostatic or hydrophobic interactions, which have been shown to determine protein adsorption to biomaterial surfaces.[46, 47] The first row of images in **Supplementary Figure 9** shows a uniform fluorescence from a silicate nanoplatelet solution. The second row (whole blood) shows blood cells with a minimal fluorescent signature. The mixture of labelled 9NC100 and PPP showed co-localization of the plasma components with the silicate nanoplatelets (third row). The same was observed for the nanoplatelets and PRP (fourth row). The uniform fluorescence of the nanoplatelets is disrupted by the presence of blood components, suggesting a change in the interactions between nanoplatelets. The co-localization of silicates and blood components is thought to originate from plasma proteins and blood cells interacting with the charged surfaces of silicate nanoplatelets, increasing blood component concentrations surrounding the nanocomposite. Earlier studies have shown that charge interactions can initiate the coagulation cascade, such as the interactions of GPIb-V receptors (negative) with platelets and von Willebrand factor (positive) with collagen.[20, 48, 49] The attractive properties of the silicates could serve to accelerate hemostasis, with similar protein–nanocomposite interactions observed in other hemostats.[45]

In vivo biocompatibility of nanocomposite hydrogels was investigated by dorsal subcutaneous injection in rats via 1 cm incisions. 9NC75 (200 µl) or QuikClot™ samples (200 µl) were injected or implanted, respectively, in subcutaneous pockets (n=16) as shown in **Figure 3a**. All animals survived the follow-up period of 28 days without any signs of physical impairment or systemic inflammation, and exhibited regular somatic growth. After 3 days, both implant materials (9NC75 and QuikClot™) could be easily detected in the subcutaneous pockets. At day 28, the QuikClot™ particles appeared macroscopically unchanged and 9NC75 was integrated in the surrounding tissue. Hematoxylin & Eosin (H&E) staining confirmed these

observations indicating that 9NC75 was predominantly degraded within 28 days after injection, while QuikClot™ did not undergo degradation (**Figure 3b**).[50] Both implants induced an acute locally restricted inflammatory reaction in the host, including cellular infiltration. This process turned into chronic inflammation of the surrounding tissue, whereas the inflammatory response against QuikClot™ was substantially stronger when compared to 9NC75, resulting in a higher density and larger area of predominantly mononuclear cellular infiltrates. Moreover, in the QuikClot™ group, dense fibrous tissue formation was detected around the implants at day 28, indicating fibrous capsule formation (**Figure 3b**).

In order to investigate the potential of the nanocomposite to stop otherwise lethal bleeding, a standardized liver bleeding model was applied (**Supplementary Figure 10**). In the liver bleeding experiments (n=12 rats), median laparotomy was performed, and the central liver lobe was exposed. After draping the surrounding *situs* with filter paper for blood collection, a circular liver laceration (1 cm diameter) with standardized shape and size was created. Immediately after the injury, 9NC75 or QuikClot™ was applied on the site of lesion. The principal lethality of this bleeding model was assessed in control animals (n=5) without application of a hemostat. Both 9NC75 (n=5) and QuikClot™ (n=2) were effective in stopping relevant hemorrhage within seconds and prevented hypovolemic conditions. A log rank analysis of the early post-interventional survival data revealed significant improvement by the nanocomposite (logrank (Mantel-Cox) test: $p=0.007$ versus control; hazard ratio 11.5 with 95% CI 1.93-68.9) (**Figure 3c**). The total blood loss after 5 and 10 minutes was significantly decreased by the application of 9NC75 ($p<0.001$ versus control) (**Figure 3d**). The small amount of applied nanocomposite (200 µl) was more than sufficient, since the superficial parts of the nanocomposite were not soaked with blood, and thorough removal of this excess material did not

cause re-bleeding (**Figure 3e**). All hemostat-treated liver bleeding animals survived the complete follow-up period of 28 days without secondary hemorrhage. At explantation, no remnants of the nanocomposite were observed and the liver presented an intact surface, while QuikClot^{TM} was still present, accompanied by soft tissue adhesion to the site of lesion. These results show that the nanocomposite gel offers a strong hemostatic potential for *in vivo* applications and is suitable to stop lethal bleeding.

In conclusion, nanocomposite hydrogels containing synthetic silicate disks and gelatin form injectable biomaterials that can promote *in vitro* and *in vivo* coagulation. The addition of silicate nanoplatelets to gelatin significantly improved the physiological stability, injectability, hemostatic performance, and nanocomposite-clot strength. Due to these unique features, the newly developed silicate based gelatin nanocomposite can be used as an injectable hemostat to treat incompressible wounds.

Methods

Materials: Synthetic silicate nanoplatelets (Laponite XLG) were purchased from Southern Clay Products, Inc. (Louisville, KY). Type-A porcine skin gelatin was obtained from Sigma Aldrich (Milwaukee, WI).

Nanocomposite Formulation: Stock solutions of 18% (w/w) gelatin and 9, 6, or 3 % (w/w) nanoplatelets were prepared in water. The nanocomposite compositions were made by vortexing the gelatin stock, nanoplatelet stock, and Milli-Q water at 3000 rpm for 5 minutes to achieve the correct solid concentration and nanoplatelet loading.

X-Ray Scattering: Small Angle X-Ray Scattering (SAXS) was performed at the NSLS at Brookhaven National Laboratory at beamline X27C. Samples were placed in a 1 mm thick washer and sealed between Kapton tape. Samples were equilibrated at 37 °C and 20 °C for 20 minutes prior to collection of data. Scattering patterns were collected for 30 seconds per sample.

Rheological Analysis: An Anton Paar MCR 301 rheometer was used for mechanical testing. A 25 mm diameter parallel plate geometry with a gap height of 500 μm was used for temperature sweeps and mineral oil was placed around the circumference of the plate to prevent evaporation of water from the nanocomposite for all tests. Nanocomposites were equilibriated for 10 minutes prior to testing, followed by a 2 minute steady shear at 10 s-1. 10 s of equilibrium time was sufficient for the viscosity to return to a higher plateau value, after which point testing was initiated. Frequency and shear rate sweeps were performed at 20 and 37 °C, with frequencies from 0.001- 100 Hz at 1% strain and shear rates from 0.001 to 100 s-1 with 10 points/decade. Frequency sweeps were performed with a cone geometry (25 mm diameter, 1° angle, 50 μm truncation gap). Stress-controlled temperature sweeps were performed from 15-45 °C at 10 Pa stress and 1 Hz. All other tests were performed at 37 °C. Oscillatory stress sweeps were

performed from 0.01-100 Pa at 1 Hz. Strain Sweeps were performed from 0.01-1000% at 1 Hz. Recovery testing was conducted at 1 Hz by applying 100% strain, a value outside of the linear viscoelastic range, followed by 1% strain for 5 minutes to monitor gel recovery. Interfacial strength was also measured by applying a linearly increasing strain to a system of nanocomposite and coagulated blood. Shear stress was measured until 1,800% strain. The maximum stress attained was used as a measure of the strength of the clot system.

Clotting Time Assay: A solution of citrated blood and 10% (v/v) 0.1 M calcium chloride ($CaCl_2$) was then added, followed by vortexing for 10 seconds. 50 μL was deposited into sequential wells on a 96 well plate. At selected time points, each well was washed with 9 g/L saline solution to halt clotting. The liquid was immediately aspirated and washes repeated until the solution was clear, indicating removal of all soluble blood components. Nanocomposites were injected via syringe into the base of the well plates prior to adding blood. Final clotting time was marked in the well that formed a uniform clot, with no change in clot size in subsequent wells.

Quantification and Imaging of Interfacial Interactions: Anticoagulated whole blood was centrifuged for 2 minutes to separate red blood cell- rich (RBC-rich) and RBC-poor phases at 6,000 rpm. A liquid solution of fluorescently labeled nanoplatelet was mixed with the RBC-rich and poor blood phases. Dilute solutions of RBC-rich/nanoplatelet and RBC-poor/nanoplatelet were mixed and deposited onto glass slides for fluorescent imaging.

In vivo experiments: Male Wistar rats (n=20; 200 – 250 g) were obtained from Charles River (Wilmington, MA, USA), housed in the local animal care facility (PRB, Cambridge, MA, USA). Anesthesia and analgesia were achieved by isoflurane inhalation (2.0-2.5%) and subcutaneous carprofen administration (5 mg/kg/d). All experiments were conducted according to the NIH

"Guide for the Care and Use of Laboratory Animals", and approved by the local animal care committee (HMA Standing Committee on Animals; protocol number 05055).

Subcutaneous Implantation: Dorsal skin incisions (1 cm in length) were conducted and a small subcutaneous pocket was generated by blunt preparation. Nanocomposite gels (n=8; 200 µl) were injected or QuikClot^{TM} samples (n=8; 200 µl) were implanted, respectively. The wounds were anatomically closed. After 3 and 28 days, the animals were euthanized by CO2 inhalation, and the implants as well as adjacent tissue were explanted and further processed for histological analyses.

Liver Bleeding: Median laparotomies were performed and the central liver lobe was exposed (n=12 rats). After draping the surrounding situs with filter paper for blood collection, a standardized circular liver laceration was created by gluing a plastic disc (d=10 mm) to the surface and superficially excising this area with a blade. Immediately after injury, nanocomposite gel (n=5; 200 µl) or QuikClot^{TM} (n=2; 200 µl) was applied on the site of lesion. Five minutes after the bleeding had been stopped, the abdomen was anatomically closed, and the animals were allowed to recover from anesthesia. After 28 days, the animals were euthanized by CO_2 inhalation, and the site of injury was inspected. In order to examine the principal lethality of the liver bleeding model, control rats (n=5) underwent liver injury without subsequent application of a hemostat. In all liver bleeding experiments, the amount of bleeding was determined by weighing filter papers used to collect lost blood after removal.

Histology: Histological analyses were conducted as previously published. In brief, paraformaldehyde-fixed cryo-sections (6 µm) of all explants were stained with hematoxylin/eosin and microscopically analyzed.[50]

References

1. Ostomel TA, Shi Q, Stucky GD. Oxide hemostatic activity. *Journal of the American Chemical Society* 2006, **128**(26)**:** 8384-8385.

2. Spotnitz WD, Burks S. Hemostats, sealants, and adhesives: components of the surgical toolbox. *Transfusion* 2008, **48**(7)**:** 1502-1516.

3. Dowling MB, Kumar R, Keibler MA, Hess JR, Bochicchio GV, Raghavan SR. A self-assembling hydrophobically modified chitosan capable of reversible hemostatic action. *Biomaterials* 2011, **32**(13)**:** 3351-3357.

4. Baker SE, Sawvel AM, Zheng N, Stucky GD. Controlling bioprocesses with inorganic surfaces: layered clay hemostatic agents. *Chemistry of Materials* 2007, **19**(18)**:** 4390-4392.

5. Ruan L, Zhang H, Luo H, Liu J, Tang F, Shi Y-K*, et al.* Designed amphiphilic peptide forms stable nanoweb, slowly releases encapsulated hydrophobic drug, and accelerates animal hemostasis. *Proceedings of the National Academy of Sciences* 2009.

6. Burnett LR, Richter JG, Rahmany MB, Soler R, Steen JA, Orlando G*, et al.* Novel keratin (KeraStat™) and polyurethane (Nanosan®-Sorb) biomaterials are hemostatic in a porcine lethal extremity hemorrhage model. *Journal of Biomaterials Applications* 2014, **28**(6)**:** 869-879.

7. Hildenbrand T. A New Gelatine-based Hemostat for Sinonasal Surgery: A Clinical Survey. *In Vivo* 2013, **27**(4)**:** 523-526.

8. Oz MC, Rondinone JF, Shargill NS. Floseal Matrix. *Journal of Cardiac Surgery* 2003, **18**(6)**:** 486-493.

9. Xie X, Tian J-k, Lv F-q, Wu R, Tang W-b, Luo Y-k*, et al.* A novel hemostatic sealant composed of gelatin, transglutaminase and thrombin effectively controls liver trauma-induced bleeding in dogs. *Acta Pharmacol Sin* 2013, **34**(7)**:** 983-988.

10. Ekenseair AK, Boere KWM, Tzouanas SN, Vo TN, Kasper FK, Mikos AG. Structure–Property Evaluation of Thermally and Chemically Gelling Injectable Hydrogels for Tissue Engineering. *Biomacromolecules* 2012, **13**(9)**:** 2821-2830.

11. Lu HD, Soranno DE, Rodell CB, Kim IL, Burdick JA. Secondary Photocrosslinking of Injectable Shear-Thinning Dock-and-Lock Hydrogels. *Advanced Healthcare Materials* 2013, **2**(7)**:** 1028-1036.

12. Ostomel TA, Shi Q, Stoimenov PK, Stucky GD. Metal oxide surface charge mediated hemostasis. *Langmuir* 2007, **23**(22)**:** 11233-11238.

13. Cha C, Shin SR, Annabi N, Dokmeci MR, Khademhosseini A. Carbon-Based Nanomaterials: Multifunctional Materials for Biomedical Engineering. *ACS nano* 2013, **7**(4)**:** 2891-2897.

14. Gaharwar AK, Peppas NA, Khademhosseini A. Nanocomposite hydrogels for biomedical applications. *Biotechnology and Bioengineering* 2014, **111**(3)**:** 441-453.

15. Schexnailder P, Schmidt G. Nanocomposite polymer hydrogels. *Colloid and Polymer Science* 2009, **287**(1)**:** 1-11.

16. Shin SR, Bae H, Cha JM, Mun JY, Chen Y-C, Tekin H*, et al.* Carbon Nanotube Reinforced Hybrid Microgels as Scaffold Materials for Cell Encapsulation. *ACS nano* 2011, **6**(1)**:** 362-372.

17. Shin SR, Jung SM, Zalabany M, Kim K, Zorlutuna P, Kim Sb*, et al.* Carbon-Nanotube-Embedded Hydrogel Sheets for Engineering Cardiac Constructs and Bioactuators. *ACS nano* 2013, **7**(3)**:** 2369-2380.

18. Dobrovolskaia MA, McNeil SE. Immunological properties of engineered nanomaterials. *Nature nanotechnology* 2007, **2**(8)**:** 469-478.

19. Jones CF, Grainger DW. < i> In vitro</i> assessments of nanomaterial toxicity. *Advanced drug delivery reviews* 2009, **61**(6)**:** 438-456.

20. Radomski A, Jurasz P, Alonso-Escolano D, Drews M, Morandi M, Malinski T*, et al.* Nanoparticle-induced platelet aggregation and vascular thrombosis. *British Journal of Pharmacology* 2005, **146**(6)**:** 882-893.

21. Semberova J, De Paoli Lacerda SH, Simakova O, Holada K, Gelderman MP, Simak J. Carbon nanotubes activate blood platelets by inducing extracellular Ca2+ influx sensitive to calcium entry inhibitors. *Nano letters* 2009, **9**(9)**:** 3312-3317.

22. Singh SK, Singh MK, Nayak MK, Kumari S, Shrivastava S, Gr√°cio JJ*, et al.* Thrombus inducing property of atomically thin graphene oxide sheets. *ACS nano* 2011, **5**(6)**:** 4987-4996.

23. Gaharwar AK, Mihaila SM, Swami A, Patel A, Sant S, Reis RL*, et al.* Bioactive Silicate Nanoplatelets for Osteogenic Diffrentiation of Human Human Mesenchymal Stem Cells. *Advanced Materials* 2013, **(25)**(24)**:** 3329–3336.

24. Ruzicka B, Zaccarelli E. A fresh look at the Laponite phase diagram. *Soft Matter* 2011, **7**(4)**:** 1268-1286.

25. Viseras C, Cerezo P, Sanchez R, Salcedo I, Aguzzi C. Current challenges in clay minerals for drug delivery. *Applied Clay Science* 2010, **48**(3)**:** 291-295.

26. Gaharwar AK, Kishore V, Rivera C, Bullock W, Wu CJ, Akkus O*, et al.* Physically Crosslinked Nanocomposites from Silicate-Crosslinked PEO: Mechanical Properties and Osteogenic Differentiation of Human Mesenchymal Stem Cells. *Macromolecular Bioscience* 2012, **12**(6)**:** 779.

27. Gaharwar AK, Rivera C, Wu C-J, Chan BK, Schmidt G. Photocrosslinked nanocomposite hydrogels from PEG and silica nanospheres: Structural, mechanical and cell adhesion characteristics. *Materials Science and Engineering: C* 2013, **33**(3)**:** 1800-1807.

28. Gaharwar AK, Schexnailder P, Kaul V, Akkus O, Zakharov D, Seifert S*, et al.* Highly Extensible Bio-Nanocomposite Films with Direction-Dependent Properties. *Advanced Functional Materials* 2010, **20**(3)**:** 429-436.

29. Gaharwar AK, Schexnailder PJ, Kline BP, Schmidt G. Assessment of using Laponite® cross-linked poly(ethylene oxide) for controlled cell adhesion and mineralization. *Acta Biomaterialia* 2011, **7**(2)**:** 568-577.

30. Arnaud F, Parreno-Sadalan D, Tomori T, Delima MG, Teranishi K, Carr W*, et al.* Comparison of 10 hemostatic dressings in a groin transection model in swine. *The Journal of Trauma and Acute Care Surgery* 2009, **67**(4)**:** 848-855.

31. Bowman PD, Wang X, Meledeo MA, Dubick MA, Kheirabadi BS. Toxicity of aluminum silicates used in hemostatic dressings toward human umbilical veins endothelial cells, HeLa cells, and RAW267. 4 mouse macrophages. *The Journal of Trauma and Acute Care Surgery* 2011, **71**(3)**:** 727-732.

32. Carretero MI, Pozo M. Clay and non-clay minerals in the pharmaceutical and cosmetic industries Part II. Active ingredients. *Applied Clay Science* 2010, **47**(3)**:** 171-181.

33. Nelson O'Donoghue M. Eye cosmetics. *Dermatologic clinics* 2000, **18**(4)**:** 633-639.

34. Ashby N, Binks B. Pickering emulsions stabilised by Laponite clay particles. *Physical Chemistry Chemical Physics* 2000, **2**(24)**:** 5640-5646.

35. Thompson DW, Butterworth JT. The nature of laponite and its aqueous dispersions. *Journal of Colloid and Interface Science* 1992, **151**(1)**:** 236-243.

36. Gaharwar AK, Schexnailder PJ, Dundigalla A, White JD, Matos-Pérez CR, Cloud JL*, et al.* Highly Extensible Bio-Nanocomposite Fibers. *Macromolecular Rapid Communications* 2011, **32**(1)**:** 50-57.

37. Wu C-J, Gaharwar AK, Schexnailder PJ, Schmidt G. Development of biomedical polymer-silicate nanocomposites: a materials science perspective. *Materials* 2010, **3**(5)**:** 2986-3005.

38. Pawar N, Bohidar H. Surface selective binding of nanoclay particles to polyampholyte protein chains. *The Journal of chemical physics* 2009, **131:** 045103.

39. Stevens KR, Einerson NJ, Burmania JA, Kao WJ. In vivo biocompatibility of gelatin-based hydrogels and interpenetrating networks. *Journal of Biomaterials Science, Polymer Edition* 2002, **13**(12)**:** 1353-1366.

40. Bohidar HB, Jena SS. Kinetics of sol-gel transition in thermoreversible gelation of gelatin. *The Journal of chemical physics* 1993, **98:** 8970.

41. Jorge MFC, Flaker CHC, Nassar SF, Moraes ICF, Bittante AMQB, Sobral PJdA. Viscoelastic and rheological properties of nanocomposite-forming solutions based on gelatin and montmorillonite. *Journal of Food Engineering* 2014, **120:** 81-87.

42. Davie EW, Ratnoff OD. Waterfall sequence for intrinsic blood clotting. *Science* 1964, **145**(3638)**:** 1310-1312.

43. de la Torre RA, Bachman SL, Wheeler AA, Bartow KN, Scott JS. Hemostasis and hemostatic agents in minimally invasive surgery. *Surgery* 2007, **142**(4)**:** S39-S45.

44. Bertram JP, Williams CA, Robinson R, Segal SS, Flynn NT, Lavik EB. Intravenous hemostat: nanotechnology to halt bleeding. *Sci Transl Med* 2009, **1**(11)**:** 11ra22.

45. Wagner WR, Pachence JM, Ristich J, Johnson PC. Comparativein VitroAnalysis of Topical Hemostatic Agents. *Journal of Surgical Research* 1996, **66**(2)**:** 100-108.

46. Roach P, Farrar D, Perry CC. Interpretation of Protein Adsorption: Surface-Induced Conformational Changes. *Journal of the American Chemical Society* 2005, **127**(22)**:** 8168-8173.

47. Wojciechowski P, Ten Hove P, Brash JL. Phenomenology and mechanism of the transient adsorption of fibrinogen from plasma (Vroman effect). *Journal of Colloid and Interface Science* 1986, **111**(2)**:** 455-465.

48. Okamoto Y, Yano R, Miyatake K, Tomohiro I, Shigemasa Y, Minami S. Effects of chitin and chitosan on blood coagulation. *Carbohydrate Polymers* 2003, **53**(3)**:** 337-342.

49. Zhang J, Xia W, Liu P, Cheng Q, Tahi T, Gu W*, et al.* Chitosan Modification and Pharmaceutical/Biomedical Applications. *Marine Drugs* 2010, **8**(7)**:** 1962-1987.

50. Assmann A, Delfs C, Munakata H, Schiffer F, Horstkötter K, Huynh K*, et al.* Acceleration of autologous in vivo recellularization of decellularized aortic conduits by fibronectin surface coating. *Biomaterials* 2013, **34**(25)**:** 6015-6026.

Acknowledgement

SAXS experiments were performed at Beamline X27C of the National Synchrotron Light Source at Brookhaven National Laboratory. This research was supported by the U.S. Army Research Office under contract W911NF-13-D-0001. RKA was supported by an NIH Interdepartmental Biotechnology Training Program (NIH/NIGMS 5T32GM008334). AP acknowledges postdoctoral award from FRQS (Fonds de recherche du Québec - Santé), Quebec, Canada. AA acknowledges a postdoctoral award from the German Heart Foundation, Frankfurt, Germany.

Author Contributions

AKG and RKA designed and performed the experiments. AP conducted cell studies and analyzed cell data. AA performed and analyzed in vivo experiments. AKG and RKA wrote the manuscript. GHM provided technical advice on rheological measurements. BDO, AK and GHM gave conceptual advice and provided comments to the manuscript.

Additional Information

Competing Financial Interests

The authors declare no competing financial interests.

Figure Legends

Figure 1: Structure, injectability, and self-healing characteristics of nanocomposite hydrogels. (a) Schematic showing the preparation of the nanocomposite gels. The TEM image shows the size of the silicate nanoparticle (Scale bar 50 nm). Images showing injection of nanocomposite hydrogel through a surgical needle (22 gauge) and recovery to form freestanding structures. (b) Zeta potential measurements demonstrate electrostatic interactions between negatively charged silicate and positively charged gelatin. 95% CI are shown for each point. (c) Small-angle X-ray scattering (SAXS) indicates that nanoplatelets are well dispersed and follow the model curve for scattering from dispersed thin disks. (d) Yield stress of gels as a function of nanoplatelet loading and solids fraction. (e) Recovery of the nanocomposites was observed by subjecting the hydrogel to alternating high and low strain conditions (100% strain and 1% strain) while monitoring the moduli of the composite. For all the nanocomposite hydrogels, more than 95% recovery was observed.

Figure 2: Effect of nanoplatelets on the clotting whole blood. (a) Clot formation as a function of time and nanocomposite composition. (b) Quantiative clot times for 6% and 9% nanocomposites. (One-way Anova followed by Tukey's post hoc analysis was performed ** $p<0.01$; *** $p<0.001$). (c) Clotting kinetics of blood when in contact with gelatin and nanocomposite monitored using shear rheology. (d) Comparison of clotting times for silicate-gelatin nanocomposite (NC) and commercial products.

Figure 3: In vivo evaluation of nanocomposite hydrogels as hemostats. (a) Subcutaneous injection and explantation of 9NC75 in rats. After 3 days, nanocomposite could be easily

detected in the subcutaneous pockets, but the volume was already lower than at implantation. (b) H&E staining confirmed degradation of 9NC75 within 28 days, while the QuikClotTM particles were still present. Moreover, 9NC75 induced less chronic inflammation than QuikClotTM, indicated by severe mononuclear cell infiltration around QuikClotTM at day 28 (asterisks). Furthermore, the QuikClotTM samples were encapsulated by dense fibrous connective tissue (arrows). The potential of the nanocomposite to stop otherwise lethal bleeding was investigated using liver bleeding experiments in rats. (c) 9NC75 significantly improved the post-interventional survival (logrank (Mantel-Cox) test). (d) 9NC75 was effective in preventing blood loss as compared to untreated hemorrhage (***$p<0.001$). (e) The small amount of 9NC75 (200 µl) was sufficient to stop bleeding and the superficial part of the 9NC75 was easily removed without causing re-bleeding.

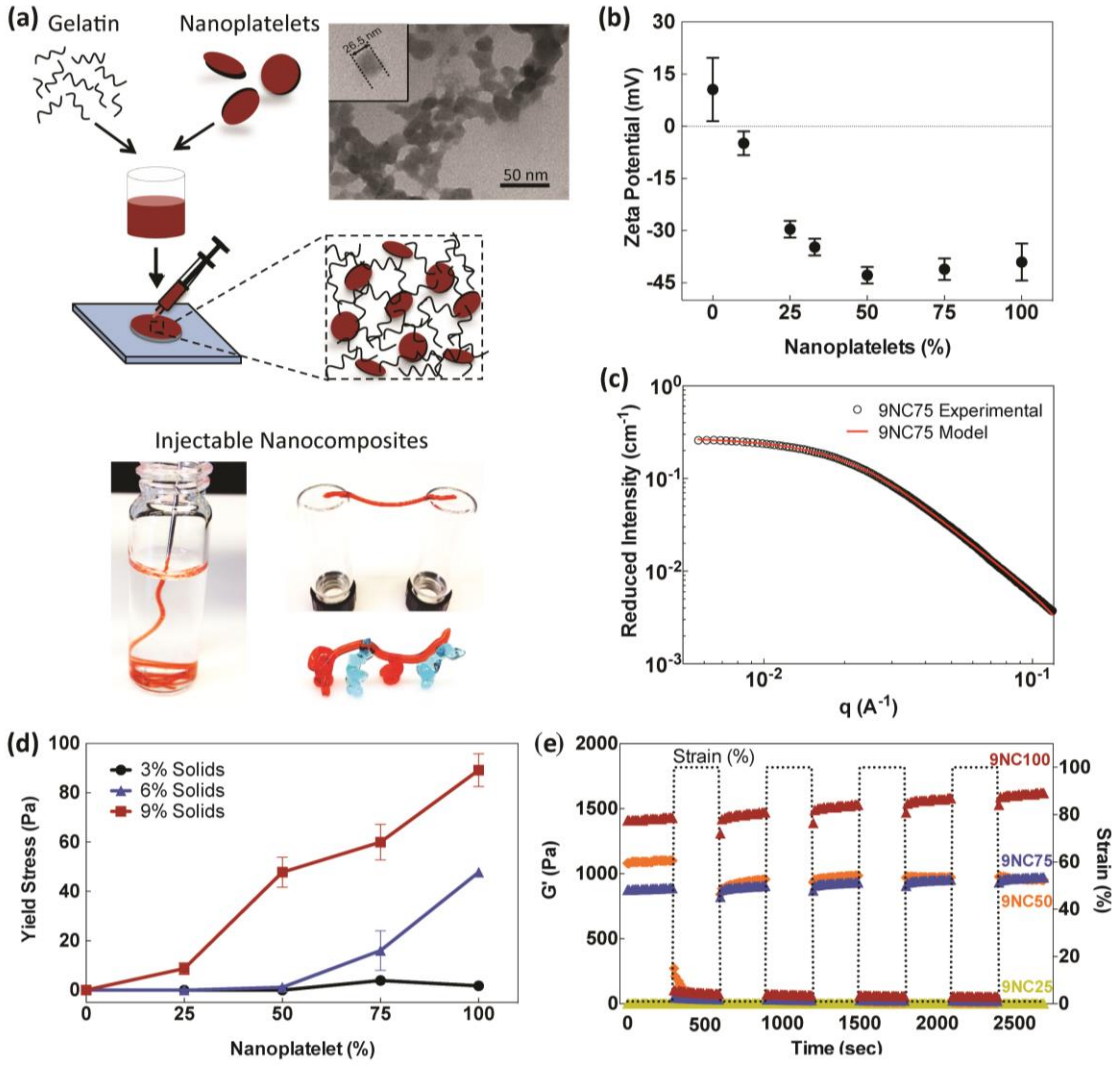
(a)
Gelatin
Nanoplatelets
26.5 nm
50 nm
Injectable Nanocomposites
(b)
Zeta Potential (mV)
Nanoplatelets (%)
(c)
9NC75 Experimental
9NC75 Model
Reduced Intensity (cm-1)
q (A-1)
(d)
3% Solids
6% Solids
9% Solids
Yield Stress (Pa)
Nanoplatelet (%)
(e)
Strain (%)
9NC100
9NC75
9NC50
9NC25
G' (Pa)
Strain (%)
Time (sec)

Figure 1

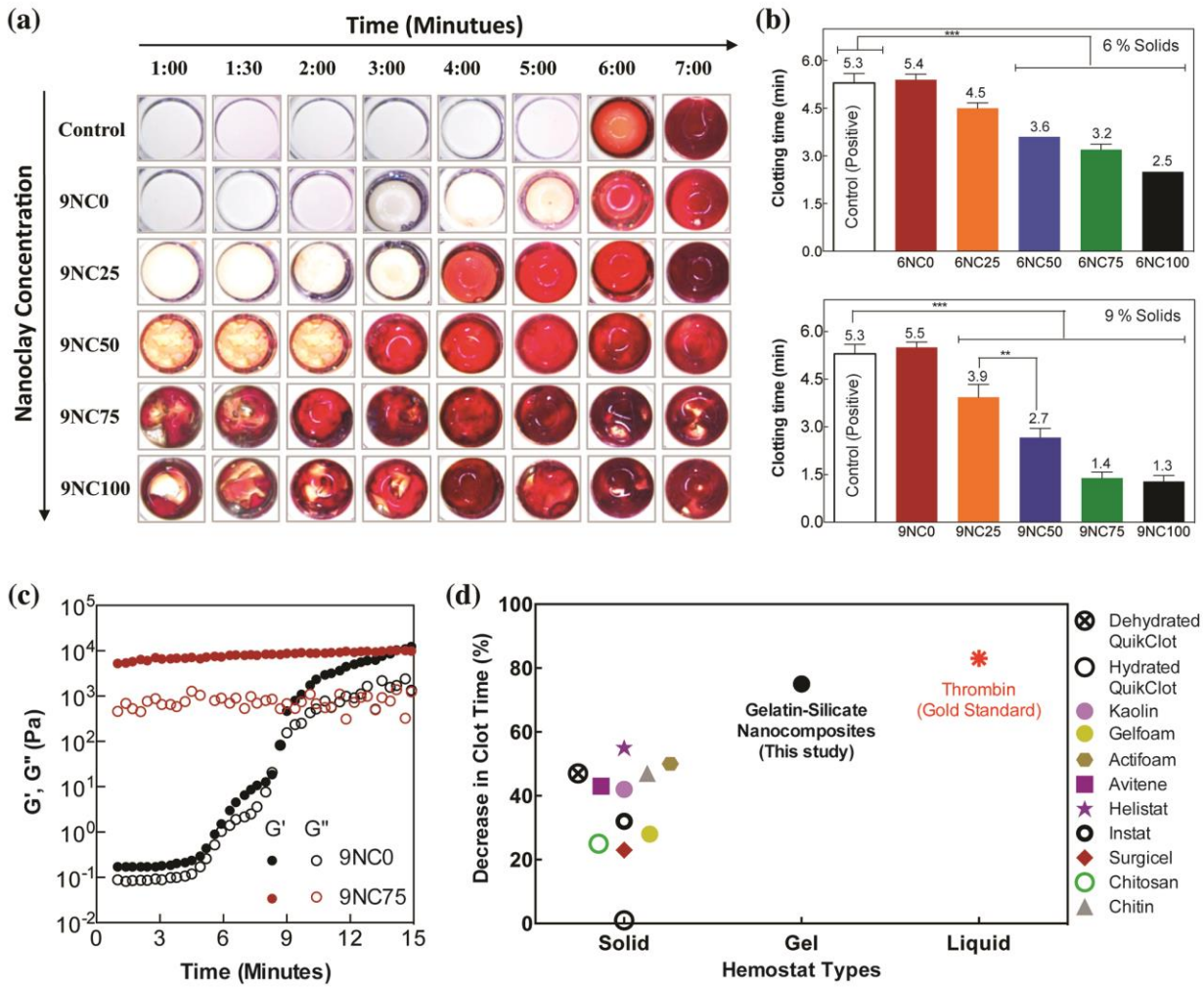
(a)
Time (Minutues)
1:00
1:30
2:00
3:00
4:00
5:00
6:00
7:00
Nanoclay Concentration
Control
9NC0
9NC25
9NC50
9NC75
9NC100
(b)
6 % Solids
9 % Solids
Clotting time (min)
Control (Positive)
5.3
5.4
4.5
3.6
3.2
2.5
5.5
3.9
2.7
1.4
1.3
6NC0
6NC25
6NC50
6NC75
6NC100
9NC0
9NC25
9NC50
9NC75
9NC100
(c)
G', G" (Pa)
G'
G"
9NC0
9NC75
Time (Minutes)
(d)
Decrease in Clot Time (%)
Gelatin-Silicate Nanocomposites (This study)
Thrombin (Gold Standard)
Solid
Gel
Liquid
Hemostat Types
Dehydrated QuikClot
Hydrated QuikClot
Kaolin
Gelfoam
Actifoam
Avitene
Helistat
Instat
Surgicel
Chitosan
Chitin

Figure 2

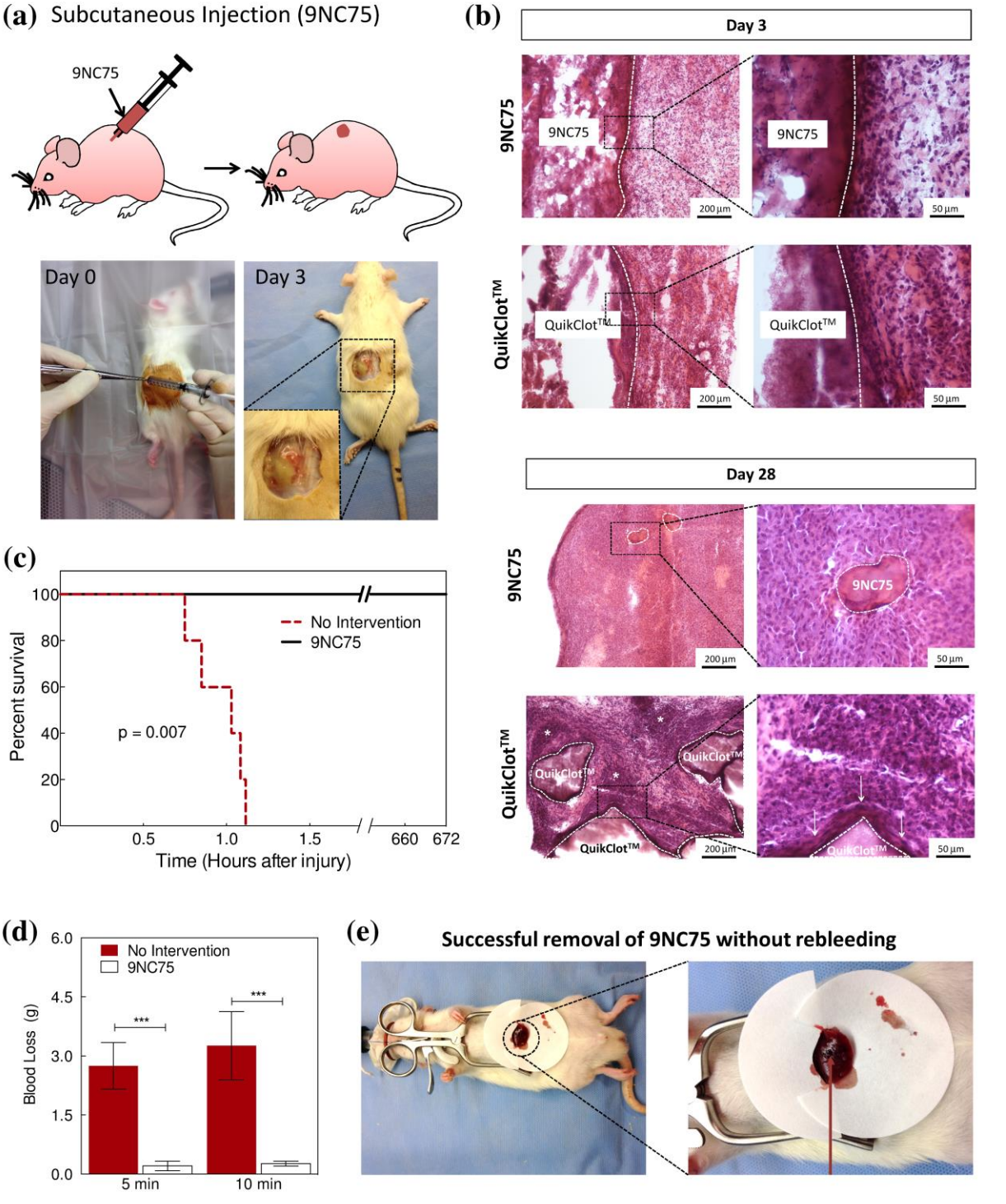
(a) Subcutaneous Injection (9NC75)
9NC75
Day 0
Day 3
(b)
Day 3
9NC75
9NC75
9NC75
200 µm
50 µm
QuikClot™
QuikClot™
QuikClot™
200 µm
50 µm
Day 28
9NC75
9NC75
200 µm
50 µm
QuikClot™
QuikClot™
QuikClot™
QuikClot™
200 µm
50 µm
(c)
Percent survival
100
80
60
40
20
0
No Intervention
9NC75
p = 0.007
0.5
1.0
1.5
660
672
Time (Hours after injury)
(d)
Blood Loss (g)
6.0
4.5
3.0
1.5
0.0
No Intervention
9NC75
***
***
5 min
10 min
(e)
Successful removal of 9NC75 without rebleeding

Figure 3

Shear-thinning Nanocomposite Hydrogels for the Treatment of Hemorrhage

Akhilesh K. Gaharwar, Reginald K. Avery, Alexander Assmann, Arghya Paul, Gareth H. McKinley, Ali Khademhosseini*, Bradley D. Olsen*

*Prof. B. D. Olsen, Dr. A. K. Gaharwar
Department of Chemical Engineering, Massachusetts Institute of Technology, Cambridge, MA 02139 (USA)
Email: (bdolsen@mit.edu)

*Prof. A. Khademhosseini, Dr. A. K. Gaharwar, Dr. A. Assmann, Dr. A. Paul
Wyss Institute for Biologically Inspired Engineering, Harvard University,
Boston, MA 02115 (USA)
Email: (alik@rics.bwh.harvard.edu)

Prof. A. Khademhosseini, Dr. A. K. Gaharwar, R. K. Avery, Dr. A. Assmann, Dr. A. Paul
Center for Biomedical Engineering, Department of Medicine, Brigham and Women's Hospital, Harvard Medical School, Cambridge, MA 02139 (USA)

Prof. A. Khademhosseini, Dr. A. K. Gaharwar, Dr. A. Assmann, Dr. A. Paul
Harvard-MIT Division of Health Sciences and Technology, Massachusetts Institute of Technology, Cambridge, MA 02139 (USA).

Dr. A. K. Gaharwar
David H. Koch Institute for Integrative Cancer Research, Massachusetts Institute of Technology, Cambridge, MA 02139 (USA)

R. K. Avery
Department of Biological Engineering, Massachusetts Institute of Technology, Cambridge, MA 02139 (USA)

Prof. G. H. McKinley
Department of Mechanical Engineering, Massachusetts Institute of Technology, Cambridge, MA 02139 (USA)

Dr. A. Assmann
Department of Cardiovascular Surgery, Heinrich Heine University, Medical Faculty, 40225 Duesseldorf (Germany)

Content

I. Additional Materials and Methods:

Materials: Zeta potentials of gelatin, silicate nanoplatelet, and mixtures of silicate and gelatin were determined in ultrapure water (Milli-Q) and phosphate buffered saline (PBS), pH 7.4 (Invitrogen) using a 633 nm laser in a Malvern ZEN3600 (Malvern Instruments, UK). Silicate nanoplatelets were dissolved with vigorous agitation (vortexing) while gelatin was dissolved with stirring at 40 °C. Transmission election microscopy (TEM) images of the silicate nanoplatelets were obtained using a JEOL JEM-1400 TEM (JEM1400) installed with a cool beam illumination system (resolution: 0.2 nm line, 0.38 nm point) and 11 megapixel Advanced Microscopy Techniques cooled charged coupled device camera at 80 kV. The sample was prepared by dispersing silicate nanoplatelets in water/ethanol solutions, placing a drop on the TEM grid, and allowing the grid to dry under vacuum.

Nanocomposite Formulation: Stock solutions of 18% (w/w) gelatin and 9, 6, or 3 % (w/w) nanoplatelets were prepared in water (**Supplementary Table 1**). Milli-Q water was heated to 40 °C to dissolve gelatin. 4 °C water was used for nanoplatelet stock solutions to retard the gelation and allow for full dissolution of nanoplatelet particles prior to gelling. The nanoplatelet gels were allowed to sit at room temperature to fully hydrate until a clear gel was formed. Nanocomposites were again heated and vortexed. The nanocomposites were then stored at 4 °C.

Nanocomposite Degradation: Nanocomposite samples were placed in 2.0 mL Eppendorf tubes and weighed. Each sample was centrifuged in a swinging bucket rotor centrifuge to obtain a flat interface. Each sample was soaked in phosphate buffered saline (pH 7.4; Invitrogen), stored at 37 °C. At set times, the PBS was removed, and the nanocomposite reweighed. The change in weight was recorded up to 24 hours after initial soaking. PBS was replaced after each weighing.

SAXS Method: Small Angle X-Ray Scattering (SAXS) was performed at the NSLS at Brookhaven National Laboratory at beamline X27C. Samples were placed in a 1 mm thick washer and sealed between Kapton tape. Samples were equilibrated at 37 °C and 20 °C for 20 minutes prior to collection of data. Scattering patterns were collected for 30 seconds per sample. Radial integration of the two dimensional scattering pattern was performed to yield a one dimensional scattering curve, which was corrected for empty cell and dark field scattering. Thin disk form factor model fitting was performed in MatLab using a nonlinear fit algorithm to fit the radius and a Gaussian distribution for polydispersity of the nanocomposite.

Thrombus Weight: Nanocomposite and powdered QuikClot™ samples were weighed into 2 mL Eppendorf tubes. Nanocomposites were centrifuged to standardize the surface area exposed. Citrated blood was reactivated by 10 % (v/v) 0.1 m $CaCl_2$. 100 µL of solution (10 µL $CaCl_2$ and 90 µL whole blood) was added to each Eppendorf tube. At each measured time point, clotting was stopped by addition of 200 µL sodium citrate solution (0.109 m). Any liquid was removed from the Eppendorf, leaving only clotted blood. The Eppendorf tubes were reweighed to determine the mass of clot produced in the tube. Clot mass was normalized to the area exposed to the nanocomposite. The same area was used for the commercial hemostat sample.

Cell Studies: Mouse monocyte/macrophage RAW 264.7 cells were procured from the ATCC. RAW 264.7 cells were grown in DMEM medium supplemented with 10% FBS and 1%

penicillin/streptomycin at 37 °C in 5% CO_2. Lipopolysaccharide (LPS) was obtained from InvivoGen. RAW 264.7 macrophages were suspended in different formulations of gelatin and silicate at a concentration of $3x10^6$ cells/ml and plated at a density of 2,000 cells/well and grown for 24h. As controls, RAW cells were untreated or treated with 100 ng/mL of LPS. An ELISA assay (SA Biosciences) was performed according to the manufacturer's protocol on the supernatants of different groups to quantify the secreted cytokines IL-6 and TNF-α by the RAW cells. In another study, the cell viability of RAW cells in the presence of gelatin and silicate for 24h was measured with Cell Titer 96 Aqueous Non- Radioactive Cell Proliferation MTS Assay (Promega) according to manufacturer's protocol using plate reader at 490 nm absorbance. In order to eliminate possible absorbance from silicate or gelatin components, the absorbance values with gelatin, silicate and nanocomposite hydrogels, without cells, was measured. These absorbance values were subtracted from the corresponding absorbance values for gelatin, silicate and nanocomposite hydrogels, with cells. This resulted in reading the absorbance values of only viable cells. Each tested hydrogel was measured in three separate wells.

II. Supplementary Tables and Figures

Supplementary Table 1: Weight percent (w/w) composition of each nanocomposite hydrogel.

Sample Name	9NC0	9NC25	9NC50	9NC75	9NC100
Gelatin (wt%)	9	6.75	4.5	2.25	0
Nanoplatelets (wt%)	0	2.25	4.5	6.75	9
Water (wt%)	91	91	91	91	91

Sample Name	6NC0	6NC25	6NC50	6NC75	6NC100
Gelatin (wt%)	6	4.5	3	1.5	0
Nanoplatelets (wt%)	0	1.5	3	4.5	6
Water (wt%)	94	94	94	94	94

Sample Name	3NC0	3NC25	3NC50	3NC75	3NC100
Gelatin (wt%)	3	2.25	1.5	0.75	0
Nanoplatelets (wt%)	0	0.75	1.5	2.25	3
Water (wt%)	97	97	97	97	97

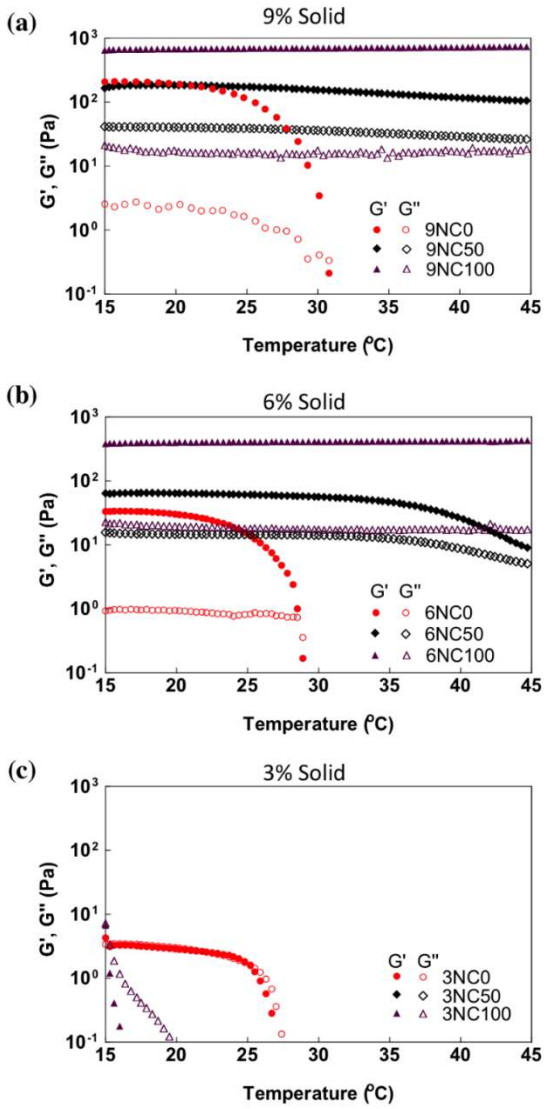

Supplementary Figure 1: Effect of silicate nanoplatelets on physiological stability of nanocomposite hydrogels. Gelatin at lower temperatures is solid, but at higher temperature it loses its mechanical integrity. Storage modulus (G') and loss modulus (G") of gelatin and nanocomposite hydrogels with solid concentrations of a) 9 wt%, b) 6 wt% and c) 3 wt% were monitored from 15 °C to 45 °C. Gelatin (NC0) was observed to flow at all solid concentrations above 32 °C. The addition of silicates improved the thermal stability of the nanocomposite network. All temperature sweeps were performed at 10 Pa stress and 1 Hz.

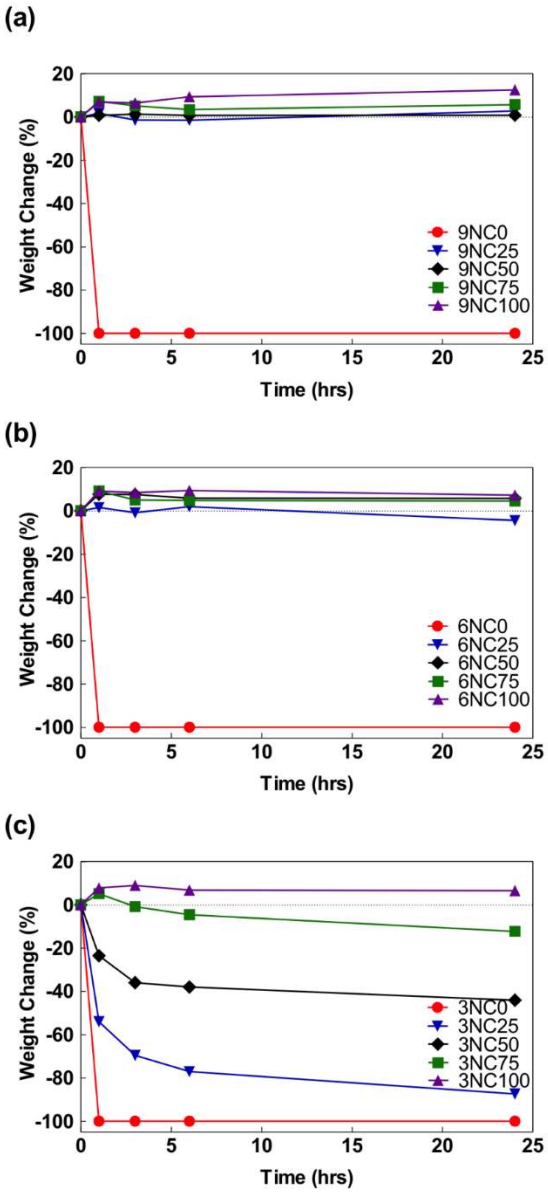

Supplementary Figure 2: Effect of silicate nanoplatelet on the stability of nanocomposite hydrogels in physiological solution. Physiological stability was determined by measuring the weight of nanocomposites with solid concentration of a) 9 wt%, b) 6 wt% and c) 3 wt% stored in PBS at 37 ºC. Gelatin (NC0) immediately dissolved in PBS, while nanocomposites of 6 wt% and 9 wt% solid concentrations maintained their structural integrity throughout the 24 hour test.

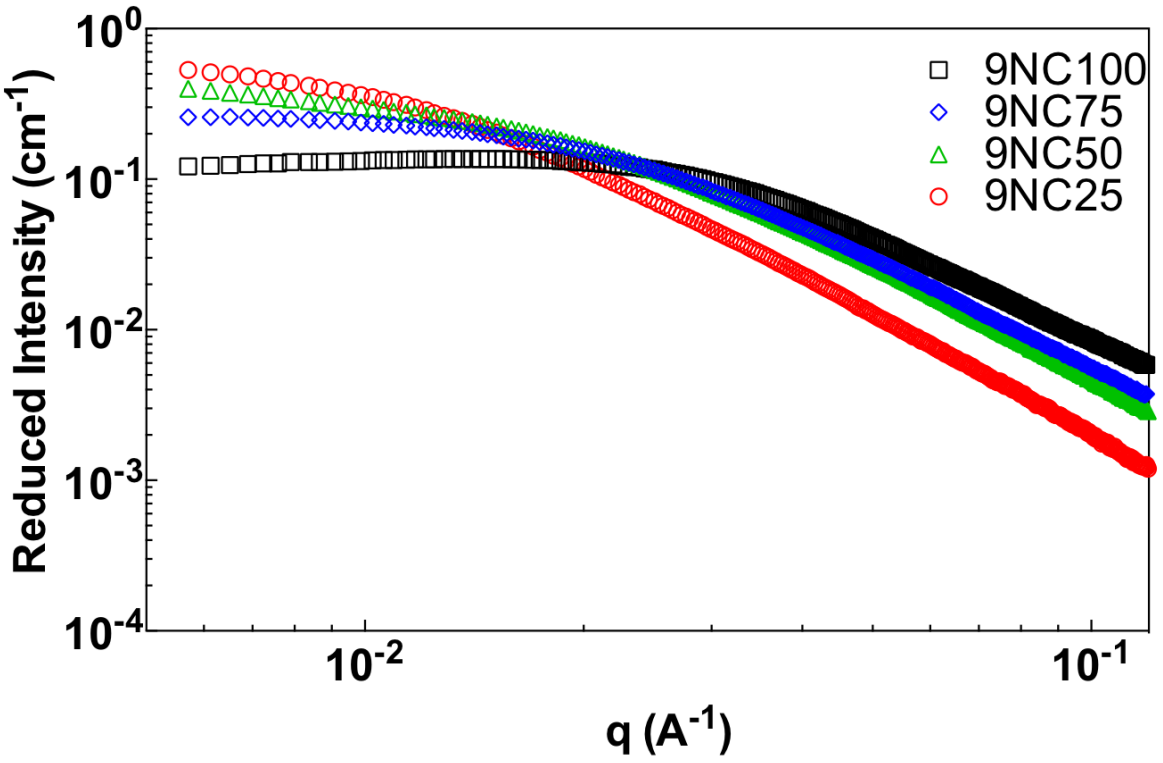

Supplementary Figure 3: X-Ray Scattering indicates disk like scatterers. SAXS intensity curves of nanocomposite samples 9NC100, 9NC75, 9NC50, and 9NC25. All samples have power law decays of exponent -2 at high q, suggesting disk shaped scatterers.

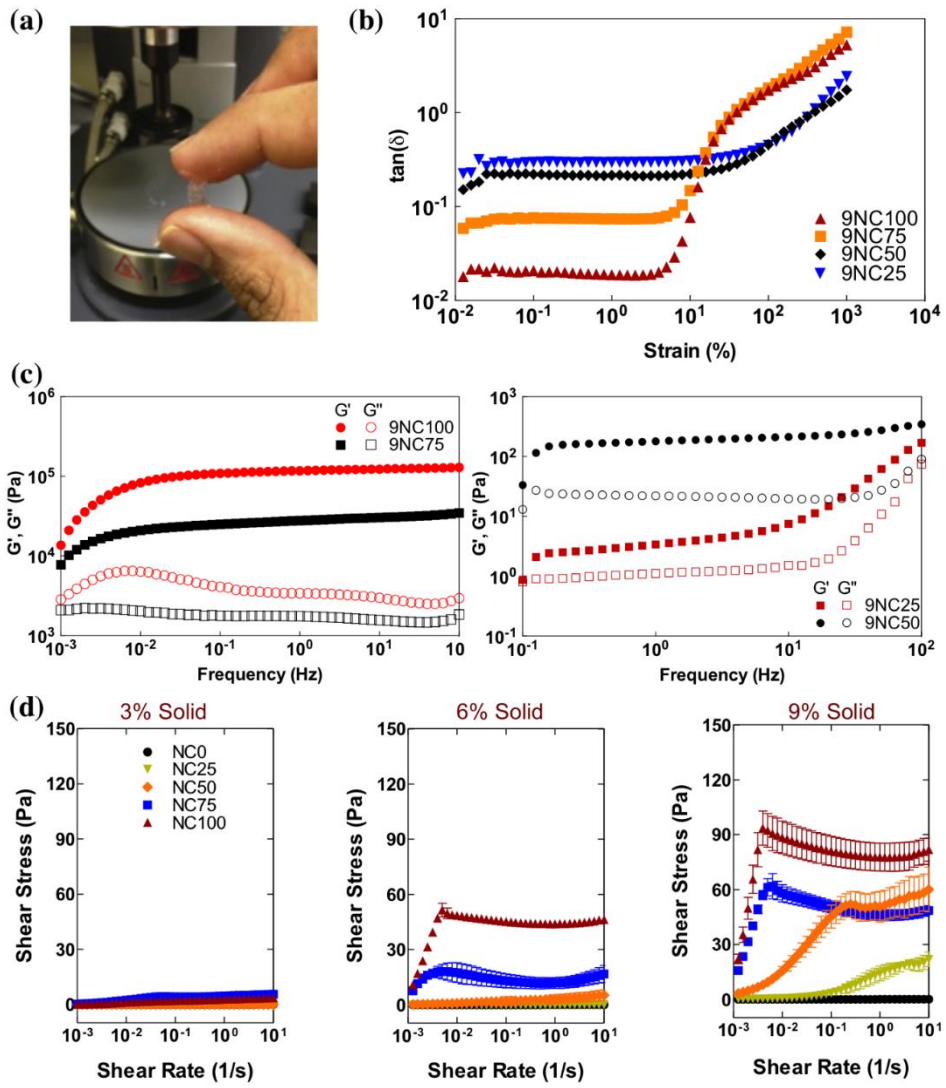

Supplementary Figure 4: Linear viscoelastic range of nanocomposite hydrogels. (a) Nanocomposites are capable of being molded and are able to maintain their shape. (b) Strain sweeps indicate a crossover point (when tan(δ) = 1) that decreases with increasing silicate loading Strain sweeps were performed at 1 Hz. (c) Frequency sweeps, at 37 °C, of 9NC25, 9NC50, 9NC75 and 9NC100 show increased moduli for higher nanoplatelet loaded nanocomposites. 9NC0 is a liquid at 37 °C and was not tested. (d) Yield stress of gels as a function of nanoplatelet loading and solids fraction (3%, 6% and 9% solid).

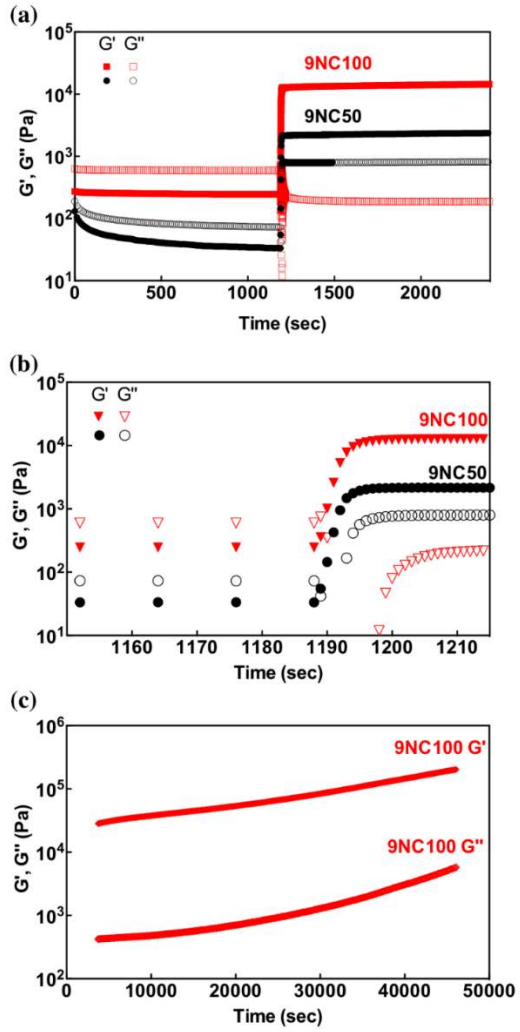

Supplementary Figure 5: Nanocomposite gel recovery and aging. Recovery tests on 9NC50 and 9NC100 show rapid recovery after high oscillatory strain. Recovery was tested by straining above the crossover point, observed from strain sweeps, to break the network, resulting in G''> G', followed by removal of the strain. The a) entire test appears as an almost instantaneous recovery to solid behavior while b) an expansion of the transition region indicates the recovery takes place within a span of 10 seconds. c) Aging was observed when samples were monitored over hours (at 1% strain, 1 Hz). This effect was able to be countered by application of high shear rates (10 s^{-1}) prior to testing, which returned moduli to their initial, non-aged values.

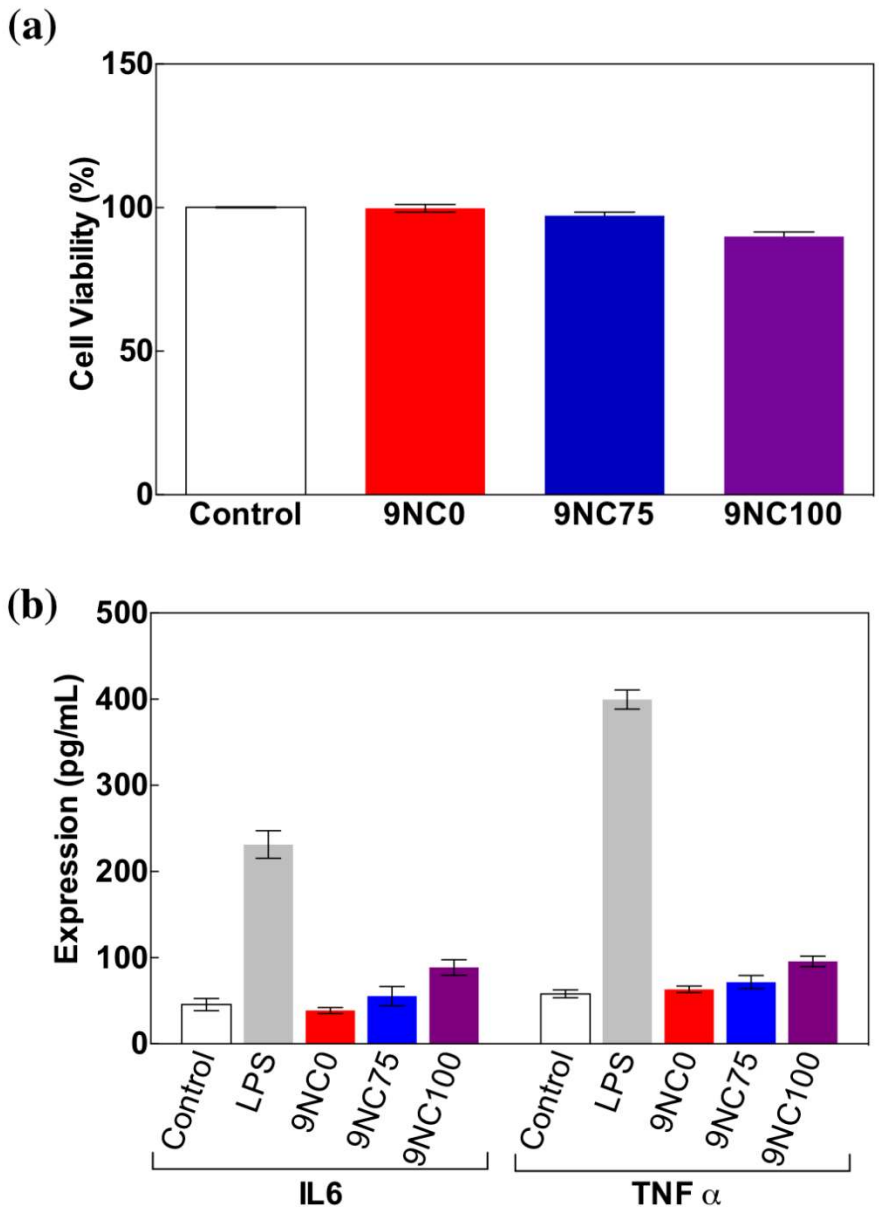

Supplementary Figure 6: Injectable Gelatin/silicate hydrogel did not induce significant cytotoxic and pro-inflammatory effects in macrophages. Toxicity profiles of gelatin (9NC0), nanoplatelet gels (9NC100), and 9NC75 with RAW macrophages as determined by a) MTS assay and b) secretion of pro-inflammatory cytokines, IL-6 and TNF-α, from RAW 264.7 macrophages after 24h of exposure.

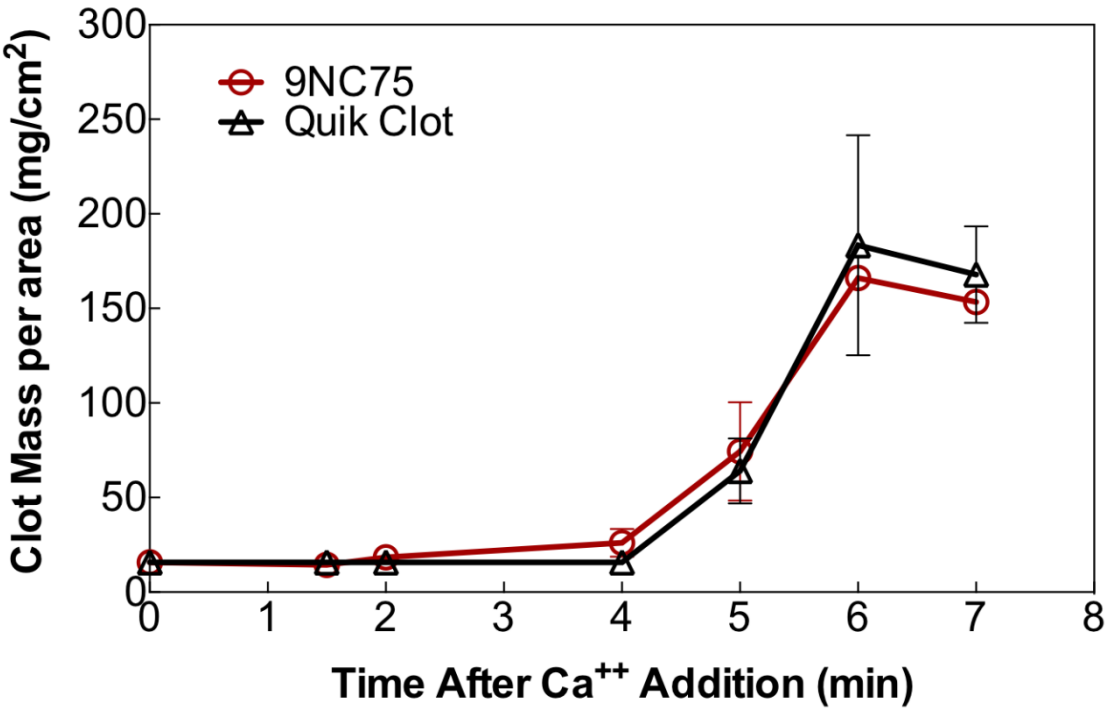

Supplementary Figure 7: Time series of clot formation. Time series of thrombus weight per area for nanocomposite and hydrated QuikClot™ powder show similar trends in the formation of a clot. The nanocomposite, an injectable system, begins to form a measureable clot at 2 minutes while QuikClot™, a solid hemostat, begins clotting at 5 minutes. Subsequent time points are not statistically different from one another, indicating that the ability of 9NC75 to form a clot is comparable to that of the commercial QuikClot™ powder. The background mass per area of 15 mg/cm^2 is due to residual liquid remaining after the washing step is performed to halt clotting.

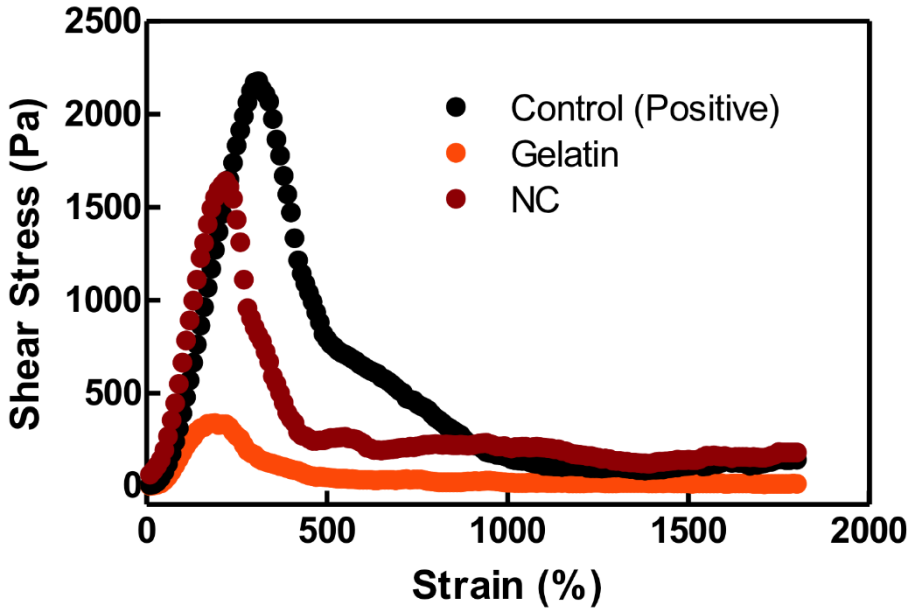

Supplementary Figure 8: Effect of nanocomposite on clot strength. Rotational strain sweep of clot and clot-nanocomposite systems show a decreased peak stress for clots in contact with 9NC0 in comparison to the peak stress of a clot alone. However, the peak stress for a 9NC75-clot system has a comparable peak stress to that of the clot alone.

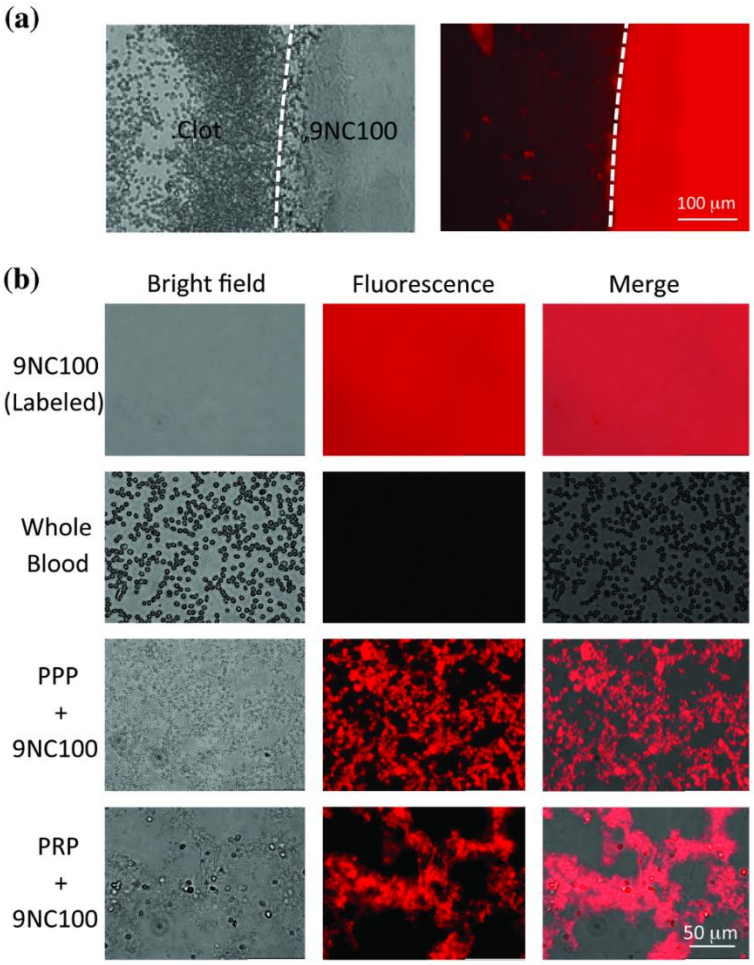

Supplementary Figure 9: Nanocomposite surface initiates clotting through interactions with blood components. (a) Fluorescent imaging reveals that the interfaces between the nanocomposite and blood have localized aggregation of RBCs. (b) Silicate nanoplatelets in contact with blood proteins and RBCs were observed using fluorescently labeled silicate nanoplatelets. The presence of blood components (platelet poor plasma (PPP) or platelet rich plasma (PRP)) in the nanoplatelets disrupt their ordering, observed by the non-uniform fluorescence signal. The stability of 9NC100, previously shown by its large absolute value of zeta potential, is decreased and aggregation occurs in systems of blood components and nanocomposites, suggesting a decrease in the zeta potential and increase in attractive forces.

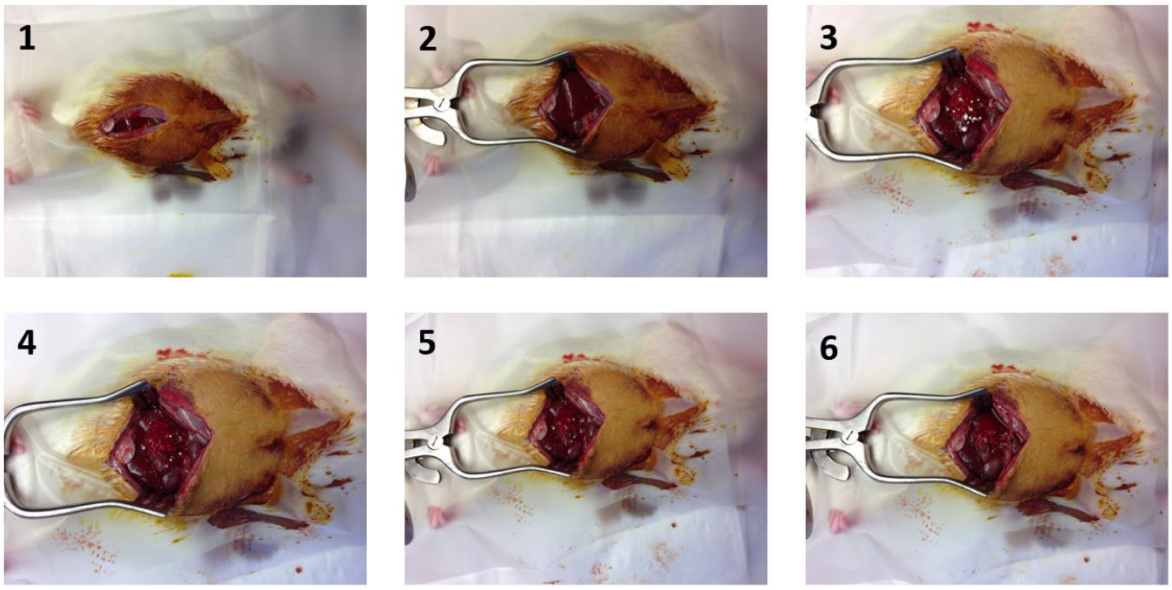

Supplementary Figure 10: *In vivo* procedure showing the liver bleeding model. To induce lethal liver bleeding, the following standardized procedure was conducted prior to re-suturing: 1) skin incision, 2) wound edge retraction to expose the liver, 3) addition of a hemostat after laceration, 4) two minutes after intervention, 5) ten minutes after intervention and 6) saline washing of the abdominal cavity. Images are from a trial with QuikClot^{TM} intervention.